HHS Public Access

Author manuscript

ACS Appl Mater Interfaces. Author manuscript; available in PMC 2019 November 07.

Published in final edited form as:

ACS Appl Mater Interfaces. 2018 September 26; 10(38): 32233–32238. doi:10.1021/acsami.8b11455.

Gas Flow at the Ultra-nanoscale: Universal Predictive Model and Validation in Nanochannels of Ångstrom-Level Resolution

Giovanni Scorrano[1,2], **Giacomo Bruno**[1], **Nicola Di Trani**[1], **Mauro Ferrari**[1], **Alberto Pimpinelli**[1,3], **Alessandro Grattoni**[1,4,5,*]

[1]Department of Nanomedicine, Houston Methodist Research Institute, Houston, Texas,77030, USA

[2]Department of Material Science and Nanoengineering, Rice University, Houston, Texas, 77005, USA

[3]Smalley-Curl Institute, Rice University, Houston, Texas, 77005, USA.

[4]Department of Surgery, Houston Methodist Hospital, Houston, Texas, 77030, USA.

[5]Department of Radiation Oncology, Houston Methodist Hospital, Houston, Texas, 77030, USA.

Abstract

Gas transport across nanoscale pores is determinant in molecular exchange in living organisms as well as in a broad spectrum of technologies. Here we report an unprecedented theoretical and experimental analysis of gas transport in a consistent set of confining nanochannels ranging in size from the ultra-nano- to the sub-microscale. A generally applicable theoretical approach quantitatively predicting confined gas flow in the Knudsen and transition regime was developed. Unlike current theories, specifically designed for very simple channel geometries, our approach can be applied to virtually all geometries, for which the probability distribution of path lengths for particle-interface collisions can be computed, either analytically or by numerical simulations. To generate a much needed benchmark experimental model, we manufactured extremely reproducible membranes with two-dimensional nanochannels. Channel sizes ranged from 2.5 to 250 nm, and Å-level of size control and interface tolerances were achieved using leading-edge nanofabrication techniques. We then measured gas flow in the Knudsen number range from 0.2 to 20. Excellent agreement between theoretical predictions and experimental data was found, demonstrating the validity and potential of our approach.

Keywords

nanochannels; convective gas flow; Knudsen regime; nanofluidic membrane

*corresponding author: agrattoni@houstonmethodist.org.

Supporting Information available including Smoluchowski equation for mean free path, probability density function from Holmin at al., membrane fabrication, and COMSOL simulation of gas flow across 250 nm membrane.

All other authors declare no competing financial interest.

1. Introduction

Numerous medical and engineering applications rely on gas flow in nanopores where the collisions of fluid molecules with confining walls dominate the characteristics of gas transport. A highly relevant example is represented by natural gas extraction from nanoporous shale rock[1]. Here, understanding nano-confined transport becomes extremely important for designing extraction techniques as well for predicting trends of gas production. Other examples are represented by gas filtration in chemical plants[2,3,4] or the development and characterization of high efficiency membranes for applications such as molecular sieving[5,6] or drug[7,8,9] and cell delivery[10,11] among others. These involve gas molecules traveling across tight spaces where the interactions with the walls are predominant as compared to the interactions among gas molecules. Furthermore, in the context of heat transport in nanoscale systems, the mean free path of a confined phonon gas is an essential ingredient in models of thermal conductivity[12]. Ideally, one can identify two limiting regimes, characterized by distinct length scales: i) A viscous regime, in which the thermal mean free path $\lambda_T \ll L_C$, where L_C is the characteristic length scale of the confining nanostructure; ii) A rarefied (free molecular flow) regime, in which $\lambda_T \gg L_C$. The latter was first investigated by Knudsen[13]. Accordingly, the Knudsen number Kn is defined as the ratio $Kn = \lambda_T / L_C$. On a finer scale, three regions can be identified: i) when $Kn < 0.1$, the gas is treated as a continuum and the Navier-Stokes equation with slip boundary condition governs gas transport[14]; ii) when $Kn > 10$, gas collisions with the confining walls dominate; this free molecular flow regime is also known as Knudsen diffusion; iii) an intermediate region, $0.1 < Kn < 10$, called transition regime, has been experimentally and theoretically explored in the literature, primarily for gases at low pressure in microfluidic systems[15]. Pressure-driven gas transport in this latter regime is characterized by the coexistence of diffusive and convective (advective) transport. As is the case for concentration driven diffusive transport[16,17], the formal description of gas flow in the transition regime in nanofluidic channels remains an open question. Surprisingly, free molecular flow is also debated: Knudsen's results rigorously apply only to gas flow inside cylindrical channels, and although his work is more than a century old, its generalization to other geometries remains controversial[18]. Experimental studies of nanoconfined gas flow are challenging, especially because of technological limitations in the fabrication of precise nanofluidic systems with a high number and density of channels and tight dimensional and geometrical tolerances. Most investigations have relied on experimental data collected with a few channels of irregular cross section, approximate size[14], and minuscule gas flow outputs[19]. Experiments adopting polymeric membranes have been limited by intricate pore geometries, poor reproducibility or high channel tortuosity[18]. A variety of porous materials such as zeolites[20], and carbon materials[21,22], such as carbon nanotubes (CNT), have received considerable attention due to their confining fluidic properties. However, their intrinsic geometric and structural variability[22] limit the investigator's ability to study the underlying transport phenomena; one can at best know the average properties of these structures, such as their average pore size - thus preventing the study of gas transport as a function of the actual Knudsen number. By leveraging leading-edge, industrial grade microfabrication techniques, we have manufactured highly accurate fluidic structures with tightly reproducible geometry, ranging in size from the ultra-nanoscale to the sub-microscale[23]. By offering an unmatched control

on channel size and geometry, such structures represent an ideal model system for the accurate investigation of the influence of geometry and size on gas transport[24] from the Knudsen to the transition regime[25].

2. Materials and Methods

2.1 Model derivation

The kinetic theory of gases allows to compute the distribution of paths of length *l* between intermolecular collisions[26] in thermal equilibrium, $p_T(l)$, whose mean value is the thermal mean free path λ_T. For a gas of identical spherical molecules of diameter d, where velocities are Maxwell-distributed at temperature T and pressure P, the thermal mean free path reads as $\lambda_T = \frac{\eta}{P}\sqrt{\frac{\pi k_B T}{2m}}$, where k_B is the Boltzmann's constant, η is the gas viscosity and m the molecular mass. It should be noted that the expectation that p_T is exponential: $p_T(l) = \exp(-l/\lambda_T)dl/\lambda_T$, is generally not true. For simplicity, we will treat it as exponential in the applications that follow. Consider a gas in a channel of rectangular section h × w and length L. When a pressure difference $\Delta P = P_{in} - P_{out}$ is applied between the channel's ends, a flux F results. Kinetic theory states that the volumetric gas flow is

$$F = D\frac{hw}{L}\frac{\Delta P}{P} = \frac{4\lambda_0\lambda_T}{3\pi\eta}\frac{hw}{L}\Delta P \quad (1)$$

where m is the molecular mass and $D = c\lambda_0/3$ is the gas diffusion coefficient written in terms of the mean thermal velocity c and the average distance between consecutive collisions, λ_0. The latter is the characteristic length that has to be computed as a function of the geometry. At Knudsen numbers Kn ≤ 1, it is expected that $\lambda_0 \approx \lambda_T$ in Eq. (1). When Kn >> 1, collisions between gas molecules can be neglected, and particle-wall encounters dominate the gas transport. In such conditions, $\lambda_0 \approx \lambda_g$, the latter being the average distance between successive collisions of a gas molecule with the channel's walls. Knudsen computed λ_g for a cylindrical geometry and showed that $\lambda_g = 2R$. He then computed λ_g for a long rectangular channel of uniform cross-section $h \times w$, where $h, w \ll L$, and found that $\lambda_g = 2hw/(h+w)$. For a gas confined between two infinite parallel plates ($w \to \infty$), $\lambda_g = 2h$. Stops[27] computed the effective mean free path in the transition regime for two infinite plates at distance h. By considering that a number of molecular paths are prematurely terminated by the boundaries, so that the effective mean free path λ_0 is less than the thermal mean free path λ_T, he computed an explicit expression, given in Eq. (8) in Stops[27]. We re-derive Stops' λ_0 and prove that his result is exact. Stops' formulation is ad hoc for the infinite parallel plates geometry; it did not consider that the geometric mean free path λ_g can be defined as the average of an appropriate distribution of path lengths, in the same way as λ_T can. Such distributions, that we call "geometric distribution of path lengths" ($p_g(l)$), are well known in the theory of the Lorentz gas,[28, 29] as well as in classical billiard dynamics. For the latter, $p_g(l)$ has been recently published by Holmin *et al.*[30] (see the full expression for a 3D box in Supporting Information Eq. S1–2).

Having defined both λ_T and λ_g as the mean values of $p_T(l)$ and $p_g(l)$, respectively, we can leverage the statistical independence of particle-wall and particle-particle collisions. Since $p_T(l)$ is the probability that a molecule collides with another molecule after traveling a distance *l*, the total probability that a molecule travels a distance *l* without collisions with other molecules is equal to $1 - \int_0^l p_T(x)dx = \int_l^\infty p_T(x)dx$. Similarly, the probability that a molecule travels a distance *l* without collisions with walls reads $\int_l^\infty p_g(x)dx$. Statistical independence guarantees that the probability of a molecule colliding with a wall but not with other molecules after traveling a distance *l* is $p_g(l)\int_l^\infty p_T(x)dx$. Interchanging the subscripts "T" and "g" yields the probability of a molecule colliding with another molecule, but not with a wall: $p_T(l)\int_l^\infty p_g(x)dx$.

2.2 Experimental setup

To test our model against experimental data, we developed and micro-fabricated several sets of nanoslit membranes, all identical except for the height h of the nanoslits. The membranes (Fig. 1) were fabricated through a sacrificial layer technique. By precisely tailoring the thickness of a tungsten film deposited by physical vapor deposition with angstrom-level resolution, slit channels with nominal heights of, respectively, 2.5, 3.5, 20, 50, 200, and 250 nm, parallel to the membrane surface (Fig. 1A) were obtained. During the fabrication process the tungsten layer represented the "space keeper" for the nanochannels. Details of the membrane fabrication are available elsewhere[23,24] and in Supporting Information. Scanning and transmission electron microscopy image analysis showed deviations from the nominal height of less than 5 Å (Fig. 1B–E). Each membrane is composed of exactly 340,252 nanochannels regularly and densely organized in rectangular arrays and connected to the membrane inlet and outlet surfaces via arrays of microchannels (Fig. 1A).

This design affords high channel density and mechanical robustness[23] and unparalleled dimensional tolerances as compared with other channel geometries. Indeed, even the most refined membranes presenting cylindrical nanopores (e.g. TiO_2 or carbon nanotubes) suffer from much poorer dimensional accuracy and manufacturing control, as well as lower scalability. We verified that despite the presence of microchannels, gas flow across our membranes is entirely dominated by the parallel set of nanochannels that represent the dominant fluidic resistance. Finite element simulations (COMSOL Multiphysics) showed that in first analysis, even for the membranes with the largest nanochannels (h = 250 nm), the pressure drop is localized between the inlet and outlet of the nanochannel region (Supporting Information Fig. S1), accounting for more than 95% for the pressure drop across the membranes, when considering entrance and exit effects.

Gas flow through silicon membranes (Fig. 1A) possessing rectangular slit-nanochannels (W = 3μm, L = 1μm, and variable h) was measured with a high sensitivity apparatus consisting in a pressure controller (PC3–15PSIG, Alicat) and three mass flow meters (M-500SCCM, M-10SCCM, M-0.5SCCM, Alicat) with different sensitivity to ensure a high signal to noise ratio always larger than 13.85 (Fig. 2). Measurements were performed by a custom-made algorithm (Matlab, The MathWorks, Inc.) setting several differential pressures from 1 to 15 psi and recording the gas flow through the silicon membrane in steady state conditions.

3. Results and Discussion

The derivation of probabilities of particle-particle and particle-wall collisions allowed us to determine the probability distribution of path lengths in a confined region of arbitrary geometry $p_g(l)\int_l^\infty p_T(x)dx + p_T(l)\int_l^\infty p_g(x)dx$, and the effective mean free path λ_0 of a gas confined in a container of arbitrary geometry:

$$\lambda_0 = \int_0^\infty l\left[p_g(l)\int_l^\infty p_T(x)dx + p_T(l)\int_l^\infty p_g(x)dx\right]dl\,. \tag{2}$$

Eq. (2) is the first important result of this paper. Eq. (2) is completely general, and for it to be useful one has to prescribe p_T and p_g. For instance, assuming both p_T and p_g to be exponential, the result $\lambda_0^{-1} = \lambda_T^{-1} + \lambda_g^{-1}$ is recovered. The calculations of the effective mean free path λ_0 in an infinite channel with rectangular cross section or in the parallel planes geometry[27] are not trivial. From Eq. (2), λ_0 can be obtained through integrations: $p_T(l)$ can be found in Paik[31] or assumed to be exponential, while $p_g(l)$ can be found in Holmin *et al.*[30] and in Supporting Information (Eq. (S1–2)). The resulting λ_0 is shown in Fig. 3 (red solid line) for a gas with thermal mean free path λ_T = 44.5 nm in a box of dimensions w = 3 μm, L = 1 μm.

Figure 3 also shows λ_g, as obtained analytically by Holmin *et al.* for a box of sides h, w and L (solid blue line): $\lambda_g = 2hwL/(hw + hL + wL)$. This coincides with Knudsen's $\lambda_g = 2hw/(h + w)$; for an infinite channel, $L \to \infty$, and that for infinite parallel planes ($w \to \infty$), $\lambda_g = 2h$. In this latter case, the geometric path distribution $p_g^\infty(l)$ can be found when w, $L \to \infty$ in the geometric path distribution of Holmin *et al.*[30] (Supporting Information Eq. (S1–2):

$$p_g^\infty(l) = \begin{cases} 0, & for\ l < h \\ \dfrac{2h^2}{l^3} & otherwise \end{cases} \tag{3}$$

Alternatively, Eq. (3) can be derived from Lambert's cosine law, $p_\theta(\theta) = 2\sin\theta\cos\theta$, together with the relations $p_g^\infty(l)\,dl = p_\theta(\theta)d\theta$, $l = h/\cos\theta$. From Eq. (3), assuming $p_T(l) = \exp(-l/\lambda_T)/\lambda_T$, and performing integrations, yields:

$$\frac{\lambda_0}{\lambda_T} = 1 - e^{-\beta} + \beta e^{-\beta} - \beta^2\int_\beta^\infty x^{-1}e^{-x}dx, \tag{4}$$

which coincides with Eq. (8) in Stops[27] where $\beta = h/\lambda_T$. Eq.(4) is also shown in Fig. 3 for comparison (dashed black line).

More complex situation can be addressed. Since Eq. (2) is an exact expression, it allows to compute the mean free path of a gas in a channel for any channel shape and wall roughness, provided $p_g(l)$ is known. In general, $p_g(l)$ has to be computed numerically, e.g. by Monte Carlo simulations which are routinely employed to evaluate the diffusion coefficient in the Knudsen regime inside channels with complicated geometries and/or rough walls. Surface

roughness was shown to lower the diffusion coefficient[32]. Thus, we propose to generalize Eq. (1) by replacing D with D' = α_0 D, and argue that the roughness-dependent α_0 plays a similar role in the definition of the accommodation coefficient of the continuum Navier-Stokes equation with Maxwell boundary conditions, when collisions with the walls are properly accounted for[33,34]. Arkilic *et al* have derived an analytical expression for gas flow through a rectangular channel, from the zero-th order solution of the compressible Navier-Stokes equation[35]. Rewriting their mass flow (Eq. (21) in Arkilic *et al.*[35]) as a volumetric flow Q, and introducing the average pressure $\bar{P} = \left(P_{in} + P_{out}\right)/2$, yields

$$Q = \frac{h^3 w}{12\eta L}\left[\frac{\bar{P}}{P_{out}} + 6\frac{2-\sigma}{\sigma}\lambda_T\right]\Delta P, \tag{5}$$

Where $(2-\sigma)/\sigma$ is the streamwise momentum accommodation coefficient. At Kn >> 1, Eq. (5) must agree with Eq. (1) when α_0 D replaces D; this implies that $\frac{2-\sigma}{\sigma} = \frac{8\alpha_0\lambda_0}{3\pi h}$, so that $\sigma = \sigma(h)$. Defining $\sigma_0 = \sigma(h=0)$, one can write explicitely:

$$\sigma(h) = \frac{4\sigma_0 h}{2\lambda_0 + \sigma_0\left(2h - \lambda_0\right)}. \tag{6}$$

From $\lambda_0 \sim 2h$ as $h \to 0$, one finds that $\alpha_0 = 3\pi\left(2-\sigma_0\right)/\left(16\sigma_0\right)$, so that for diffusively reflecting walls, $\sigma_0 = 1$ implies $\alpha_0 \approx 0.589$. We can therefore rewrite Eq. (5) as follows:

$$Q = \frac{h^3 w}{12\eta L}\left[\frac{\bar{P}}{P_{out}} + 3\frac{2-\sigma_0}{\sigma_0}\frac{\lambda_0(h)\lambda_T}{h^2}\right]\Delta P. \tag{7}$$

Equation (7) is the second important result of the present work, because only Navier-Stokes equations with geometry-dependent accommodation coefficient are able to reproduce experimentally observed Knudsen minimum in the channel permeability $q = \frac{3\pi}{8}\frac{L}{h^2 w}\frac{\bar{P}}{\Delta P}\frac{Q}{\sqrt{RT}}$.

We demonstrate this in Figure 4 where the results of permeability as a function of $\delta = 1/\mathrm{Kn}$ are shown. Figure 4 displays Eq. (5) in Arkilic *et al*[35] with $\sigma = \sigma_0 = 1$ (dashed black line), our model Eq.(7) with $\sigma_0 = 1$ (solid red line), as well as the permeability computed by Cercignani *et al.*[36] for the Boltzmann equation (solid blue line). The Navier-Stokes equation with constant accommodation coeffcients, Eq. (5), reproduces both the small h (large Kn) and the large h (small Kn) limits, but fails to exhibit a minimum around Kn ≈ 1. Cercignani et al.'s solution to the Boltzmann equation shows the expected minimum, at the expense of an unphysical divergence at small h. This is a well-known drawback of the linearized Boltzmann equation with (geometry-independent) Maxwell boundary conditions. This divergence is enhanced in the limit of entirely specular reflection: for free molecular flow, the flow rate diverges even faster as σ_0 decreases. In contrast, our Eq. (7) satisfies all requirements with a simple analytical expression adaptable to any channel geometry.

The volumetric gas flows measured at ΔP varying between 1 and 15 psi or at varying nanochannel size (ΔP =15 psi) are represented in Figure 5A and B, respectively. Results are shown for membranes with h = 2.5, 3.5, 20, 50, 200, 250 nm (n=30 replicate measurements), where the standard deviation (always < 7%) is smaller than the size of data marks. Plotted lines are Eq. (7) with $\sigma_0 = 1$. Striking agreement between the experimental data and our model (Eq. 7) was found for all values of h, which is remarkable considering that no free parameters were used.

Although other works considered a geometry-dependent mean free path in the boundary conditions[34,35], our approach has the distinct advantage to provide a systematic way of computing the mean free path in a channel with any geometry. As $p_T(l)$ is known, one only needs to compute the path length distribution $p_g(l)$, which is only determined by wall-wall collisions and can be evaluated numerically for arbitrary geometry. The geometry-dependent effective mean free path λ_0 can then be computed from Eq. (2) to any desired accuracy, and from the latter, the geometry-dependent accommodation coeffcient can be obtained. Inserting the latter in the Navier-Stokes equation (5), the volumetric flow for the entire span of Kn can be quantitatively predicted, as with (7).

4. Conclusions

In this paper we developed a statistical model for the calculation of the effective mean free path that takes into account particle-particle and particle-wall collisions. The nanochannel membranes employed in this work, also have unique characteristics: they achieved the high standard of accuracy and reproducibility, unmatched in the literature to date, allowing us to reliably test our statistical approach to nanoconfined gas transport. The remarkable agreement between model and experiments validated both. Such compelling outcomes is of great interest for numerous applications: in the natural gas industry our predictive model could provide a valuable tool to improve extraction from shale formations and tight sands[37], where gas is trapped in complex networks of micro- and nanopores. Refined modeling of gas flow in shale fractures could lead to increased yield, efficiency and environmental safety of gas recovery. For analytical technologies, a better description of gas transport across chromatography columns could lead to more efficient instrumentation and reduced time of analysis. Further application examples include nanofluidics for the detection of chemical agents, membranes for physical separation of gases in the chemical industry, analysis of confined fluids[17,38] and controlled drug release[39,40,41,42].

Supplementary Material

Refer to Web version on PubMed Central for supplementary material.

Acknowledgements

The authors are grateful to Thomas Geninatti, Giulia Rizzo for their help on the experimental results, and to Arturas Ziemys for precious discussions. The author thank Virginia Facciotto (virginia.facciotto@gmail.com) for the graphic design of schematics. Funding support from NIH NIGMS (R01 GM 127558) and CASIS (GA-2013–118, GA-2014–145). Membranes provided by NMS. M.F. disclose a financial interest in NanoMedical Systems, Inc., Austin, Texas.

References

(1). Wu T; and Zhang D Impact of Adsorption on Gas Transport in Nanopores. Sci. Rep. 2016, 6, 33461.

(2). Ding L; Wei Y; Li L; Zhang T; Wang H; Xue J; Ding L-X; Wang S; Caro J; Gogotsi Y MXene Molecular Sieving Membranes for Highly Efficient Gas Separation. Nat. Commun. 2018, 9, 155. [PubMed: 29323113]

(3). Park HB; Kamcev J; Robeson LM; Elimelech M; Freeman BD Maximizing the Right Stuff: the Trade-off between Membrane Permeability and Selectivity. Science, 2017, 356, eaab0530.

(4). Sholl DS and Lively RP Seven Chemical Separations to Change the World. Nature, 2016, 532, 435–437. [PubMed: 27121824]

(5). Tong HD; Jansen HV; Gadgil VJ; Bostan CG; Berenschot E; van Rijn CJM; Elwenspoek M Silicon Nitride Nanosieve Membrane. Nano Lett. 2004, 4, 283–287.

(6). Chang N; Gu Z-Y; Wang H-F; Yan X-P Metal–Organic-Framework-Based Tandem Molecular Sieves as a Dual Platform for Selective Microextraction and High-Resolution Gas Chromatographic Separation of N -Alkanes in Complex Matrixes. Anal. Chem. 2011, 83, 7094–7101. [PubMed: 21800908]

(7). Sih J; Bansal SS; Filipini S; Ferrati S; Raghuwansi K; Zabre E; Nicolov E; Fine D; Ferrari M; Palapattu G; Grattoni A Characterization of Nanochannel Delivery Membrane Systems for the Sustained Release of Resveratrol and Atorvastatin: New Perspectives on Promoting Heart Health. Anal. Bioanal. Chem. 2013, 405, 1547–1557. [PubMed: 23090650]

(8). Ferrati S; Nicolov E; Zabre E; Geninatti T; Shirkey BA; Hudson L; Hosali S; Crawley M; Khera M; Palapattu G; Grattoni A The Nanochannel Delivery System for Constant Testosterone Replacement Therapy. J. Sex. Med. 2015, 12, 1375–1380. [PubMed: 25930087]

(9). Filgueira CS; Nicolov E; Hood RL; Ballerini A; Garcia-Huidobro J; Lin JZ; Fraga D; Webb P; Sabek OM; Gaber AO; Philips KJ; Grattoni A Sustained Zero-Order Delivery of GC-1 from a Nanochannel Membrane Device Alleviates Metabolic Syndrome. Int. J. Obes. 2016, 40, 1776–1783.

(10). Farina M; Chua C; Ballerini A; Thekkedath U; Alexander J; Rhudy J; Torchio G; Fraga D; Pathak R; Villanueva M; Shin C; Niles J; Sesana R; Demarchi D; Sikora A; Acharya G; Gaber A; Nichols J; Grattoni A Transcutaneously Refillable, 3D-Printed Biopolymeric Encapsulation System for the Transplantation of Endocrine Cells. Biomaterials, 2018, 177, 125–138. [PubMed: 29886385]

(11). Farina M; Alexander J; Thekkedath U; Ferrari M; Grattoni A Cell Encapsulation: Overcoming Barriers in Cell Transplantation in Diabetes and Beyond. Adv. Drug Deliv. Rev. 2018, doi: 10.1016/j.addr.2018.04.018.

(12). Ju YSand Goodson KE Phonon Scattering in Silicon Films with Thickness of Order 100 nm. Appl. Phys. Lett. 1999, 74, 3005–3007.

(13). Knudsen M Die Molekularströmung der Gase durch Offnungen und die Effusion. Ann. Phys. 1909, 333, 999–1016.

(14). Roy S; Raju R; Chuang HF; Cruden BA; Meyyappan M Modeling Gas Flow through Microchannels and Nanopores. J. Appl. Phys. 2003, 93, 4870–4879.

(15). Ewart T; Perrier P; Graur IA; MeOlans JG Mass Flow Rate Measurements in a Microchannel, from Hydrodynamic to near Free Molecular Regimes. J. Fluid Mech. 2007, 584, 337–356.

(16). Bruno G; Di Trani N; Hood R; Zabre E; Filgueira CS; Canavese G; Jain P; Smith Z; Demarchi D; Hosali S; Pimpinelli A; Ferrari M; Grattoni A Unexpected Behaviors in Molecular Transport through Size-controlled Nanochannels down to the Ultra-nanoscale. Nat. Commun. 2018, 9, 1682; [PubMed: 29703954]

(17). Grattoni A; Gill J; Zabre E; Fine D; Hussain F; Ferrari M Device for Rapid and Agile Measurement of Diffusivity in Micro- and Nanochannels. Anal. Chem. 2011, 83, 3096–3103. [PubMed: 21434670]

(18). Gruener S and Huber P Knudsen Diffusion in Silicon Nanochannels. Phys. Rev. Lett. 2008, 100, 064502.

(19). Maurer J; Tabeling P; Joseph P; Willaime H Second-Order Slip Laws in Microchannels for Helium and Nitrogen. Phys. Fluids 2003, 15, 2613–2621.

(20). Tomita T; Nakayama K; Sakai H Gas Separation Characteristics of DDR Type Zeolite Membrane. Microporous Mesoporous Mater. 2004, 68, 71–75.

(21). Kim HW; Yoon HW; Yoon S-M; Yoo BM; Ahn BK; Cho YH; Shin HJ; Yang H; Paik U; Kwon S; Choi JY; Park HB Selective Gas Transport Through Few-Layered Graphene and Graphene Oxide Membranes. Science 2013, 342, 91–95. [PubMed: 24092738]

(22). Cooper SM; Cruden BA; Meyyappan M; Raju R; Roy S Gas Transport Characteristics through a Carbon Nanotubule. Nano Lett. 2004, 4, 377–381.

(23). Fine D; Grattoni A; Hosali S; Ziemys A; De Rosa E; Gill J; Medema R; Hudson L; Kojic M; Milosevic M; Brousseau L III; Goodall R; Ferrari M; Liu X A Robust Nanofluidic Membrane with Tunable Zero-Order Release for Implantable Dose Specific Drug Delivery. Lab. Chip 2010, 10, 3074. [PubMed: 20697650]

(24). Grattoni A, De Rosa E, Ferrati S, Wang Z, Gianesini A, Liu X, Hussain F, Goodall R, Ferrari M, Analysis of a Nanochanneled Membrane Structure through Convective Gas Flow. J. Micromechanics Microengineering 2009, 19, 115018.

(25). Karniadakis G; Beskok A; Gad-el-Hak M Micro Flows: Fundamentals and Simulation. Appl. Mech. Rev. 2002, 55, B76.

(26). Visco P; van Wijland F; Trizac E Collisional Statistics of the Hard-sphere Gas. Phys. Rev. E 2008, 77, 041117.

(27). Stops DW The Mean Free Path of Gas Molecules in the Transition Régime. J. Phys. Appl. Phys. 1970, 3, 685–696.

(28). Lorentz HA Le Mouvement des Electrons dans les Métaux. Arch. Neerl. 1905, 10, 336.

(29). Bourgain J; Golse F; Wennberg B On the Distribution of Free Path Lengths for the Periodic Lorentz Gas. Commun. Math. Phys. 1998, 190, 491–508.

(30). Holmin, S.; Kurlberg, P.; Mansson, D. https://arxiv.org/abs/1702.08096, 2017.

(31). Paik ST Is the Mean Free Path the Mean of a Distribution?. Am. J. Phys. 2014, 82, 602–608.

(32). Russ S; Zschiegner S; Bunde A; Kärger J Lambert Diffusion in Porous Media in the Knudsen Regime: Equivalence of Self-diffusion and Transport Diffusion. Phys. Rev. Lett. E 2005, 72, 030101.

(33). Arlemark EJ; Dadzie SK; Reese JM An Extension to the Navier–Stokes Equations to Incorporate Gas Molecular Collisions with Boundaries. J. Heat Transfer 2010, 132, 041006–1.

(34). Guo ZL; Shi BC; Zheng CG An Extended Navier-Stokes Formulation for Gas Flows in the Knudsen Layer near a Wall. Europhys. Lett. 2007, 80, 24001.

(35). Arkilic EB; Schmidt MA; Breuer KS TMAC Measurement in Silicon Micromachined Channels. Rarefied Gas Dyn. 1997, 20, 6.

(36). Cercignani C; Lampis M; Lorenzani S Variational Approach to Gas Flows in Microchannels. Phys. Fluids 2004, 16, 3426–3437.

(37). Javadpour F; Fisher D; Unsworth M Nanoscale Gas Flow in Shale Gas Sediments. J. Can. Pet. Technol. 2007, 46, 55.

(38). Bruno G; Geninatti T; Hood RL; Fine D; Scorrano G; Schmulen J; Hosali S; Ferrari M; Grattoni A Leveraging Electrokinetics for the Active Control of Dendritic Fullerene-1 Release across a Nanochannel Membrane. Nanoscale 2015, 7, 5240–5248. [PubMed: 25707848]

(39). Ferrati S; Nicolov E; Bansal S; Zabre E; Geninatti T; Ziemys A; Hudson L; Ferrari M; Goodall R; Khera M; Palapattu G; Grattoni A Delivering Enhanced Testosterone Replacement Therapy through Nanochannels. Adv. Healthc. Mater. 2015, 4, 446–451. [PubMed: 25274059]

(40). Ferrati S; Nicolov E; Bansal S; Hosali S; Landis M; Grattoni A Docetaxel/2-Hydroxypropyl β-cyclodextrin Inclusion Complex Increases Docetaxel Solubility and Release from a Nanochannel Drug Delivery System. Curr. Drug Targets 2015, 16, 1645–1649. [PubMed: 25706254]

(41). Filgueira CS; Bruno G; Chua C; Ballerini A; Folci M; Gilbert AL; Jain P; Sastry JK; Nehete PN; Shelton KA; Hill LR; Ali A; Youker KA; Grattoni A Efficacy of Sustained Delivery of GC-1 from a Nanofluidic System in a Spontaneously Obese non-Human Primate: a Aase Study. Biomed. Microdevices, 2018, 20, 49. [PubMed: 29916059]

(42). Chua CYX; Jain P; Folci M; Ballerini A; Rhudy J; Gilbert A; Singh S; Bruno G; Filgueira CS; Yee C; Butler EB; Grattoni A Nanofluidic Drug-eluting Seed for Sustained Intratumoral Immunotherapy in Triple Negative Breast Cancer. Journal of Controlled Release, 2018, 285, 23–34. [PubMed: 30008369]

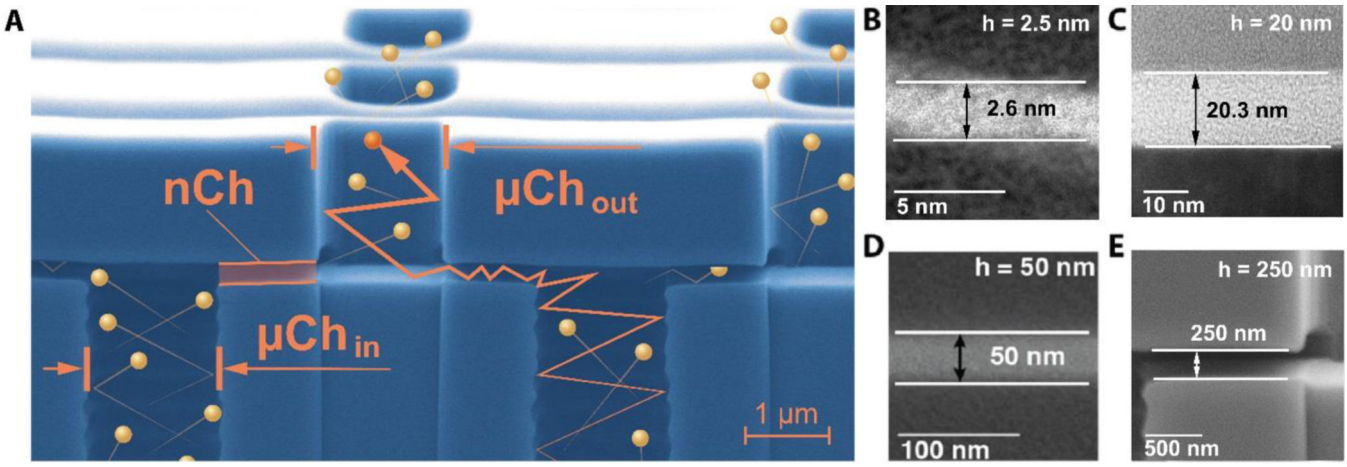

Figure 1:

Schematic depiction of the membrane structure (A); TEM cross-sectional images of selected membranes (B, C, D, E); see text for details.

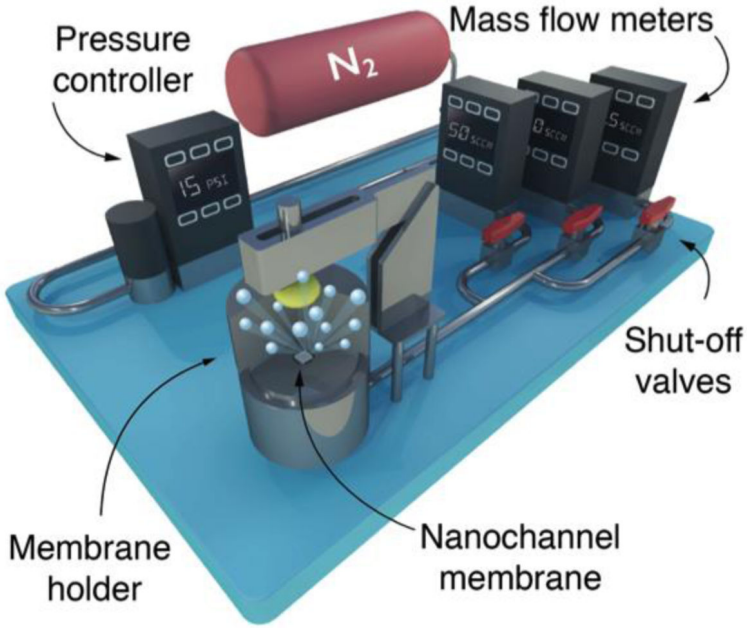

Figure 2.
Schematics of the high sensitivity apparatus developed for mass flow measurements.

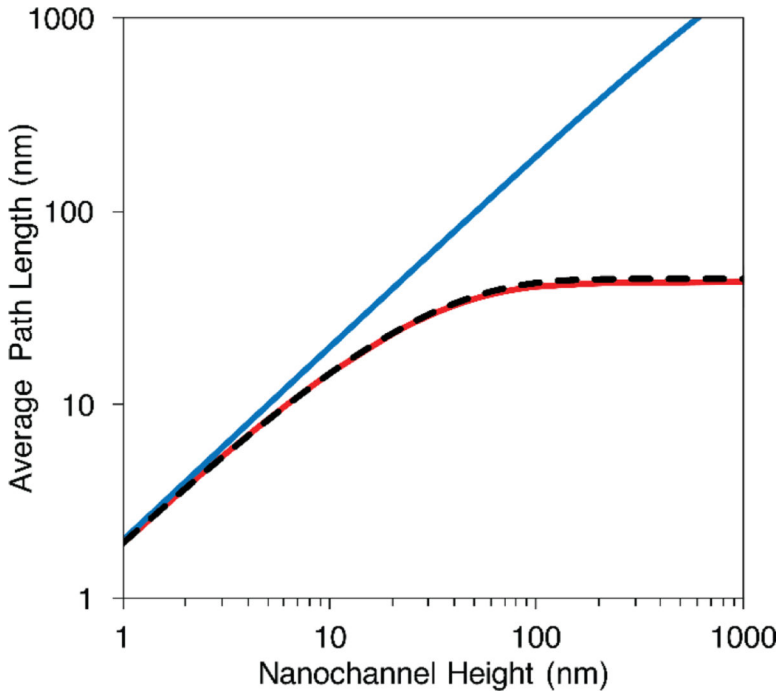

Figure 3.

Comparison of mean free path variation for the present model (solid red line), results from Stops (dashed black line), and Knudsen's model (solid blue line).

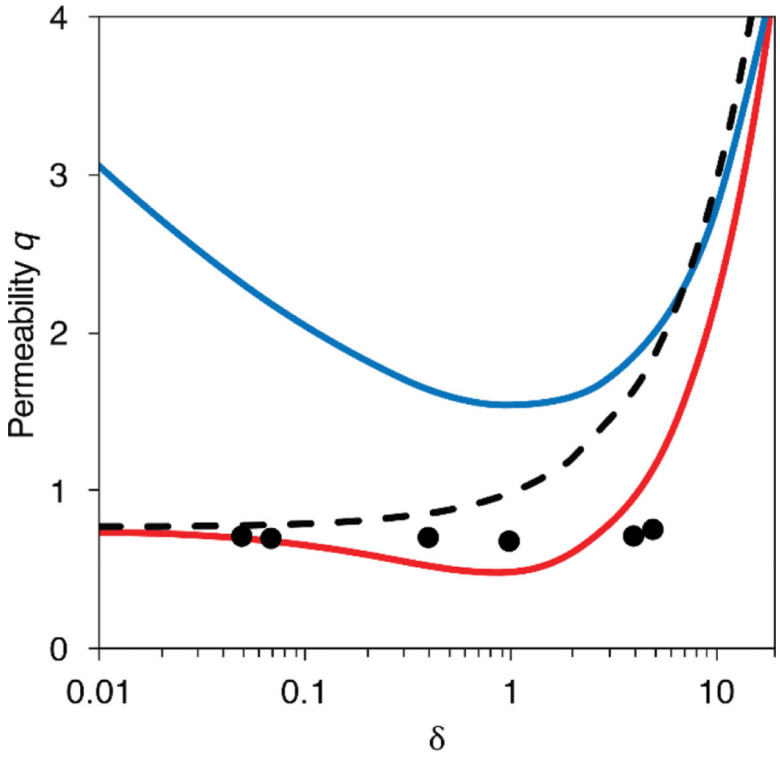

Figure 4.

Permeability calculated for Eq. (7) of the present model (solid red line), for Cercignani's solution of Boltzmann equation (solid blue line), for Arkilic model from Eq. (5) (dashed black line), and experimental data at ΔP =15 psi (black dots) as a function of the rarefaction parameter δ=1/Kn.

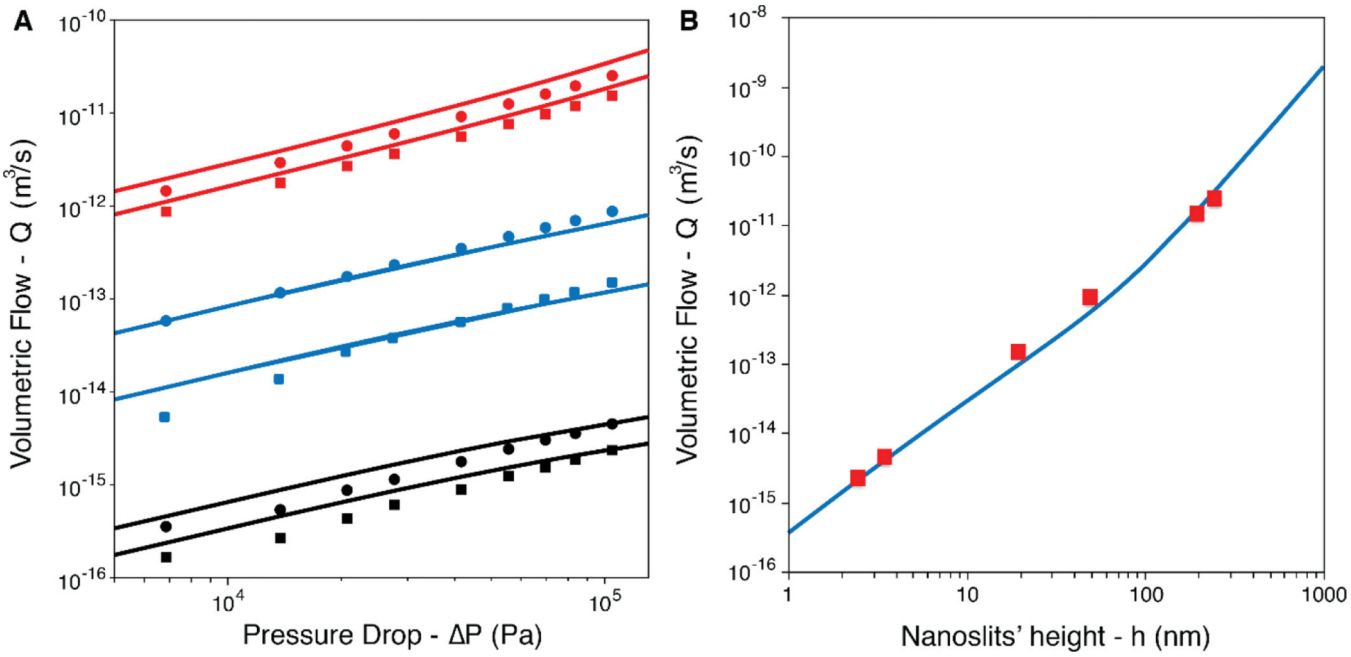

Figure 5.

(A) Volumetric gas flow Q as a function of ΔP for membranes with h = 2.5 (black squares), 3.5 (black circles), 20 (blue squares), 50 (blue circles), 200 (red squares), 250 (red circles) nm, respectively. The solid lines represent Eq. (7) for the considered values of h. (B) Volumetric nitrogen flow at ΔP =15 psi as a function of the nanochannel height.